Proximal sensing mapping method to generate field maps in vineyards

Verónica Sáiz-Rubio, Francisco Rovira-Más

(*Agricultural Robotics Laboratory*, *Polytechnic University of Valencia*, *Spain*)

Abstract: An innovative methodology to generate vegetative vigor maps in vineyards (*Vitis vinifera* L.) has been developed and pre-validated. The architecture proposed implements a Global Positioning System (GPS) receiver and a computer vision unit comprising a monocular charge-coupled device (CCD) camera equipped with an 8-mm lens and a pass-band near-infrared (NIR) filter. Both sensors are mounted on a medium-size conventional agricultural tractor. The synchronization of perception (camera) and localization (GPS) sensors allowed the creation of globally-referenced regular grids, denominated universal grids, whose cells were filled with the estimated vegetative vigor of the monitored vines. Vine vigor was quantified as the relative percentage of vegetation automatically estimated by the onboard algorithm through the images captured with the camera. Validation tests compared spatial differences in vine vigor with yield differentials along the rows. The positive correlation between vigor and yield variations showed the potential of proximal sensing and the advantages of acquiring top view images from conventional vehicles.

Keywords: precision viticulture, proximal sensing, machine vision, GPS, vigor map, yield map, NIR

Citation: Sáiz-Rubio, V. , and F. Rovira-Más. 2013. Proximal sensing mapping method to generate field maps in vineyards. Agric Eng Int: CIGR Journal, 15(2): 47−59.

1 Introduction

The availability of site-specific crop information brings many advantages to producers, especially if this information is accessible early enough to help in strategic decisions before harvesting time. Getting key information about crop status facilitates giving right treatments at the precise time (Blackmore, 2000). Many Precision Agriculture (PA) applications have been studied to provide crucial information to producers by presenting the results on field maps (Godwin and Miller, 2003; Baluja et al., 2012; Bramley and Williams, 2001; Best et al., 2011). In particular, vineyards (*Vitis vinifera* L.) are favorable to vision sensing because of the high reflectance of vegetation when compared to the rest of elements found in the field (Gausman, 1977), and vine vigor has been well correlated to the important parameters such as grape production or yield (Hall et al., 2002). In addition, wine grapes have an added value in its final produce; the wine, which favors the adoption of new technology. The narrow band of the spectrum where healthy vegetation possesses such a high reflectance rate, typically called the vegetation red edge (Weekley, 2007), is located between 700 nm and 800 nm. The red edge has been studied in isolation and also combined with other narrow bands of the electromagnetic spectrum (Chaerle and Van der Straeten, 2000). This property of crops has been helpful in multiple applications within the framework of precision farming, such as the discrimination of grape varieties (Lacar et al., 2001), the detection of nitrogen deficiency in crops (Noh et al., 2005), the assessment of water content in fields (Alchanatis et al., 2006), and the estimation of nitrogen stress in plants (Kim et al., 2001). Multispectral and hyperspectral techniques have been widely used in remote sensing to study vine vigor due to the advantages

Received date: 2012-07-20 **Accepted date:** 2013-03-21
Corresponding author: Verónica Sáiz-Rubio, Ph.D student, Agricultural Robotics Laboratory, Polytechnic University of Valencia. Email: vesairu@upvnet.upv.es.

of its high radiometric quality to estimate biomass in vineyards with the purpose of detecting zones of different productivity within a field (Lamb et al., 2001; Lamb et al., 2004). Vine vigor has been related to important crop parameters to build yield maps (Godwin and Miller, 2003), quality control maps of fertilizer applications (Giles and Downey, 2001), or diseases, infestations, and grape maturity maps (Johnson et al., 2003). Similarly, Johnson et al. (2000), and Johnson et al. (2001) used remote sensing to divide fields in equally-mature zones where differential harvesting could be applied. According to Bramley et al. (2011a) and Bramley et al. (2011b), harvesting a field through different stages separated in time in such a way that only those clusters at the optimum conditions are collected (selective harvesting) is an effective strategy to improve wine quality; and consequently detecting the best moment to harvest grapes in zones of different properties is essential to discriminate diverse quality rates among the yield and eventually make supreme quality wines (Best et al., 2011; Johnson et al., 2003). Unfortunately, multispectral applications from remote sensing techniques may not be affordable to the average wine producers in Europe -usually smallholders - who need to face major technical and economical adversities. Rovira-Más (2010), Sáiz-Rubio and Rovira-Más (2012), and Bramley et al. (2011c) have recently highlighted multiple advantages of ground sensing, also known as proximal sensing, where the possibility of adapting conventional vehicles to extract critical information while the vehicle is executing other field tasks makes this alternative very attractive for farm managers. In a similar fashion, McCarthy et al. (2010) pointed out the suitability of ground sensing in vineyards as these crop fields have wide planting frameworks and, normally, wide space among rows, which allows a correct visualization of vines and vehicle driving. Furthermore, Taylor et al. (2005) proposed a change in optical systems from remote to ground imagery in order to improve the estimation of vine vigor, and Bramley et al. (2007) confirmed this fact by taking more accurate images for determining vegetation coverage. Praat et al. (2004) also implemented a ground-based machine vision system to quantify vegetation in vineyards, but the need to attach bulky structures to the vehicle to control image parameters has made this approach impractical in the field. Interestingly, some commercial devices based on proximal sensing have been recently released, but their cost and lack of flexibility in the application to different crops have discouraged their general adoption by producers. One of the crucial challenges related to image-based sensing of vegetation is the variable reflectance distribution derived from sun-angle variations along the day and camera attitude changes along the rows, a phenomenon measured by the bidirectional reflectance distribution function (BRDF). Ground-based measurements revealed that sun-angle variations affected Normalized Difference Vegetation Index (NDVI) values depending on the observer's (camera) position (Schopfer et al., 2007); and Eklundh et al. (2011) encouraged researchers to test their vegetation monitoring systems in off-nadir positions, confirming Kimes's results (1983) which proved that nadir viewing increased vegetation reflectance with the increasing off-nadir view angles.

With the objective of overcoming some of the difficulties mentioned above regarding costs and accessibility to crop information, the research reported in this article tries to make information technology available to the average wine producer by mounting sensors and processors on conventional agricultural vehicles and proposing moderately priced systems for field mapping.

2 Materials and method

The architecture proposed for vigor mapping was evaluated through several field tests carried out with a standard tractor (JD 5820, Deere Co., Moline, IL, USA) equipped with its proprietary global positioning system (GPS) receiver StarFire^{TM} (SF) iTC featuring ±25 cm precision (SF1 free signal). The antenna of the SF receiver was centered on the vehicle's cabin as indicated by Figure 1. Additionally, an alternative low-cost GPS receiver (Garmin 18x - 5Hz, Olathe, KS, USA) was affixed to the camera supporting arm as a redundant sensor with an error inferior to 3 m. The imaging sensor of the mapping engine was a charge-coupled device (CCD) camera, monocular and monochrome (JAI,

Copenhagen, Denmark), with an 8-mm lens (Goyo Optical Inc., Saitama, Japan) coupled to a pass-band near infrared (NIR) filter BP880 (Midwest Optical Systems, Inc., Palatine, IL, USA) centered at 880 nm. Over the tests, the camera acquired and saved images at an average rate of 1.8 frames per second and the tractor traveled at average speeds of 5 - 6 km h^{-1}. A laptop computer (2.20 GHz and 1.5 GB of RAM) was used to run the mapping software especially programmed for this application. The complete system architecture is shown in Figure 1, where the camera was set to visualize the row of vines situated on the left side of the tractor. The position of the camera was such that its image plane was kept approximately parallel to the ground, resulting in top view images captured at 2.7 m above the ground and about 1.5 m above vegetation.

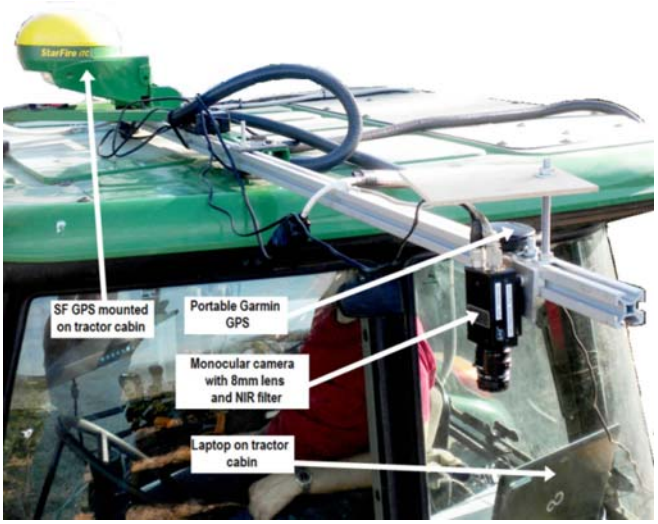

Figure 1 Mapping system mounted on the experimental tractor used in the field tests

The field tests performed to build vigor maps took place in the vineyards of a winery located in the wine production region of Utiel-Requena (Valencia, Spain), over the seasons of 2010 and 2011. Eight rows of a 20-year-old Cabernet-Sauvignon grape vine planted on a 1.5 m height trellis and an irrigated clay-limestone soil were selected to carry out the field experiments. The testing rows were approximately 120 m long and row spacing was 3 m, as is shown in the image of Figure 2b. Figure 2a plots the trajectories followed by the tractor to cover the selected eight rows - labeled 2 to 9 in the Figure - during the field tests. The sensor configuration of Figure 1 always keeps the perceived row on the left of the tractor, and therefore on the left of the GPS-recorded trajectory when the vehicle moves forward, as indicated in Figure 2a by the arrows specifying the travel direction of the tractor. In order to make driving easier and maneuvering time shorter, the recording passes were driven alternatively according to the sequence of rows 2, 6, 3, 7, 4, 8, 5 and 9, as depicted in Figure 2a.

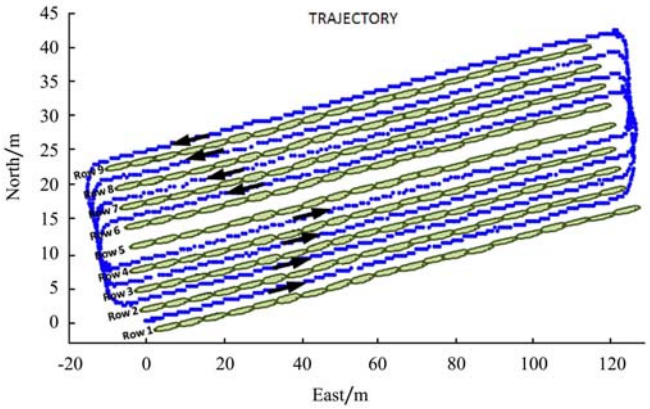

A. Path followed by the vehicle

b. Actual field

Figure 2 Field experiments

A multiplicity of lenses with different focal lengths (6, 8, 12, 16 and 25 mm), optical filters (NIR, ultraviolet (UV), NIR + UV), digital cameras (monochrome and color), and camera positions on the vehicle were combined along the field experiments with the purpose of identifying the set of parameters and setups that best met the initial objectives. The optimum configuration for estimating vigor in vines turned out to be the assemblage of the camera on the aluminum bar affixed to the cabin roof shown in Figure 1; which set the monochrome camera looking downwards with an 8 mm lens and a NIR

filter. This camera arrangement provided a top view of the plants that enhanced their perception and facilitated the application of image processing algorithms. The resolution of the images was set to 696 pixels (H) by 520 pixels (V), which covered an area of 1,190 mm by 889 mm when the separation of the camera and the canopy was around 1.5 m.

2.1 Image processing

When reflectance from healthy plants is sensed in the NIR band of the spectrum with an imaging sensor, a grey level disequilibrium occurs in the images as a consequence of the high reflectance rate exerted by vegetation, which appears atypically whiter than in regular monochrome images captured in the visible range (Knipling, 1970). These "unbalanced" images constitute the basic entry of the methodology proposed, and consequently their proper generation is vital for the success of the segmentation algorithm. The core of the automatic segmentation engine is the *Segmentation Profile* curve (Sáiz-Rubio and Rovira-Más, 2012), whose archetypical form is depicted in Figure 3. The abscissas axis of the segmentation profile represents the 256 levels of grey belonging to 8-bit images, specifically ranging from h = 0 (black) to h = 255 (white), and the ordinate axis provides the percentage of pixels $P(h)$ whose grey level is higher than the grey level considered in the abscissas axis. The NIR-forced unbalance of the images usually leads to either bright pixels representing vegetation or dark pixels coming from the non-vegetal background. This particular situation results in a drastic drop of the segmentation profile around specific grey levels which establish the boundary levels between vegetation and the rest of objects in the image. The objective of the algorithm that will automatically quantify vegetation is the detection of this drop in the profile curve for each image acquired. The best estimate of the drop position in the abscissa axis will be considered the segmentation threshold μ that will separate vegetation from non-vegetation. The curve drop was found by means of two mathematical concepts: the *gradient* (Equation (1)) and the *curvature* (Equation 2). Equation (1) provides an estimation of the gradient, $\Delta(h)$, applied to the segmentation profile, where for grey level h, the difference in segmentation profile is applied according to Equation (1), being δ the resolution of the gradient estimation in terms of increments of grey level. In the algorithm implemented in the tractor, the magnitude of δ ranged from 1 to 50 levels. The segmentation profile $P(h)$ can be defined as the percentage of pixels in the image with grey level superior to h.

$$\Delta(h) = \nabla(h) \cdot \delta = | P(h) - P(h+\delta) |;$$
$$h = 0...255 - \delta;\ \delta = 1...50 \quad (1)$$

$$\Delta^2(h) = \nabla^2(h) \cdot \delta = | \Delta(h) - \Delta(h+\delta) |;$$
$$h = 0...255 - 2\delta;\ \delta = 1...50 \quad (2)$$

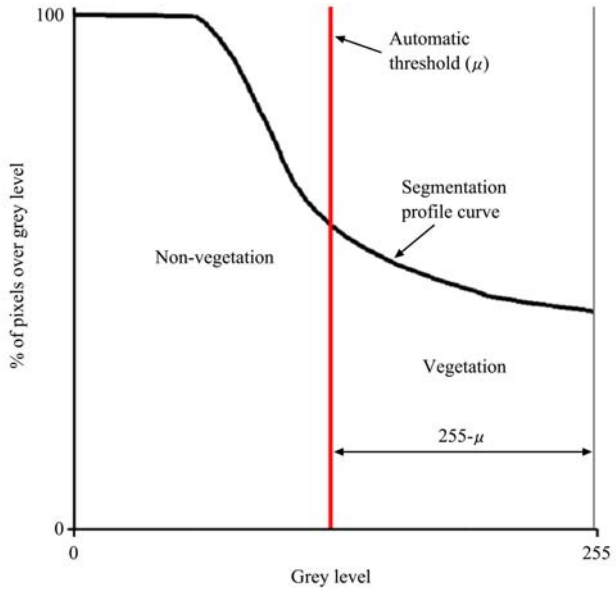

Figure 3 Segmentation profile and automatic calculation of the threshold

The estimation of the curvature on the profile was another indicator used to detect the drastic drop of the segmentation profile. The mathematical expression of the curvature encoded in the algorithm is defined in Equation (2), where $\Delta^2(h)$ is the estimation of curvature in the profile at grey level h for an interval δ. Note that the application of Equation (2) requires the previous estimation of the gradient $\Delta(h)$. The final expression for $\Delta^2(h)$ is based on the simplification usually performed on the conventional definition of curvature presented in Equation (3), where y would represent percentages of segmented pixels $P(h)$, x would correspond to grey levels h, κ is the curvature, and y' is the first derivative of y.

$$\kappa = | y'' | / (1 + y'^2)^{3/2} \approx | d^2 y / dx^2 | \quad (3)$$

Finally, the optimum threshold μ was defined as the average of the grey levels that maximized $\Delta(h)$ and $\Delta^2(h)$, symbolized by h_Δ and respectively, and corrected by the offset λ as is shown in Equation (4). The threshold μ indicates the approximate location in the segmentation profile where the highest drop occurs. The offset λ was empirically adjusted in the field and ranged from 0 to 50 grey levels.

$$\mu = \lambda + (h_\Delta + h_{\Delta 2}) / 2;\ \lambda = 0....50 \quad (4)$$

Figure 3 represents the segmentation profile of a random image saved by the onboard algorithm in one of the passes. When the segmentation engine was set to work in automatic mode, the thresholds μ calculated by the algorithm with Equation (4) were drawn in the corresponding curves saved by the onboard computer. After each threshold μ had been determined, the algorithm segmented the equivalent original images by changing to black all the pixels considered as non vegetation by the algorithm; and leaving the rest of the pixels - considered vigorous vegetation - with their original levels of grey. As a final point, the algorithm counted vegetation pixels and calculated the percentage of the image covered by vegetation.

The customized software used in the field, and run in real time, can be conceptually divided into two core algorithms simultaneously executed in the onboard computer; one to manage the perception system (monocular camera) and the other to handle the global localization engine (GPS receivers). A third algorithm devoted to the generation of global maps was implemented in the map building computer, generally off-line and off-vehicle. The ultimate objective of the entire three-algorithm procedure was the construction of information maps with high interest for PA applications such as vine vigor maps or yield (either predicted or measured) maps of vineyards. Figure 4 is a block diagram that describes how the three main algorithms manage and exchange fundamental information to fulfill the final objective of storing crop data through global maps. According to Figure 4, the user initiates the mapping process by turning the camera on to start image acquisition from the perception algorithm, but before saving any information, the image parameters of resolution (δ), exposure time (shutter speed), offset (λ), and illumination gain need to be manually adjusted to current environmental conditions. Once these four parameters have been set, the camera starts saving sequences of NIR images so that the vision algorithm can calculate automatic thresholds, and estimate local variations of vigor. As indicated in Figure 4, both the segmented images and the profile curves can be displayed and recorded at any moment. In addition to visual information, thresholds and vegetation percentages were stored in a text file. Simultaneous to the execution of the perception algorithm, the localization engine continuously provided the global coordinates of the vehicle in order to associate every image to a position in the field. The instantaneous position of the vehicle was initially given in geodetic coordinates latitude, longitude, and altitude. However, these coordinates are not convenient for the representation of maps in agriculture where fields are mostly flat and small when compared to the size of the earth. The ideal alternative is brought by the Local Tangent Plane (LTP) coordinate system, which features Euclidean geometry, allows user-set origins, and employs the intuitive coordinate frame east-north (Grewal et al., 2001; Rovira-Más et al., 2011). The transformation between coordinate systems took place in real time inside the localization algorithm, but not every point in the field was paired with an image; raw messages received by the GPS in National Marine Electronics Association (NMEA) code were constantly analyzed for consistency and only those considered reliable provided the images with a position in the field. All the images associated to unreliable positions were discarded as their contribution to the global map deteriorated it by adding wrong data. The consistency check implemented in the algorithm assured that the number of satellites in solution was above four and the horizontal dilution of precision (HDOP) was always acceptable. Nevertheless, these two conditions were not sufficient to grant the precise localization of the mapping vehicle and a more sophisticated filtering routine had to be implemented in the localization algorithm encoded in the onboard computer (Rovira-Más and Banerjee, 2012).

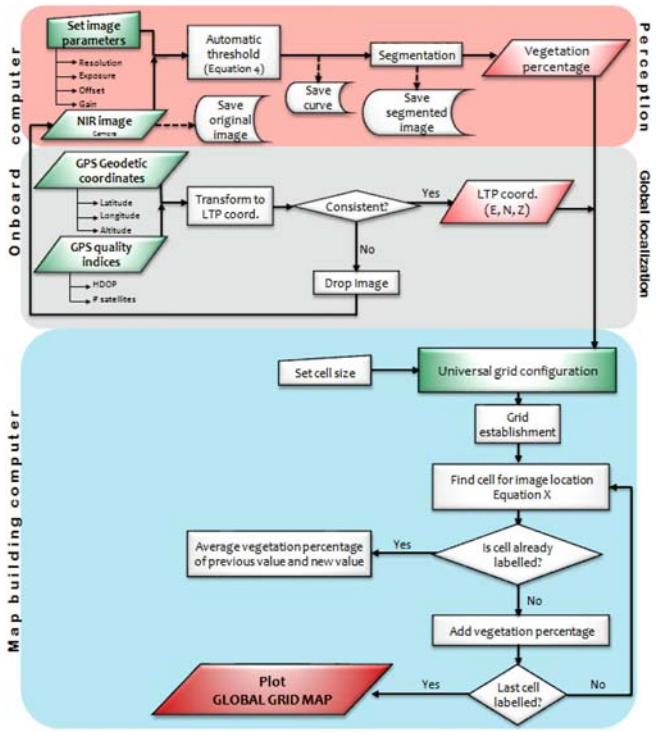

Figure 4 Block diagram of the three algorithms encoded in the mapping vehicle to create vigor maps

Unlike the perception and localization algorithms that were executed in real time during the mapping missions, the mapping algorithm was run in the laboratory after the vehicle finished the acquisition of field data. To assemble a grid-based global map of plant vigor, the mapping algorithm required two essential inputs: the instantaneous percentage of vegetation estimated from the images and the LTP coordinates of the positions where vigor was sensed. The former entry was provided by the perception algorithm after processing NIR images, and the latter was the output of the GPS receiver after conditioning its data strings. Figure 4 highlights the inputs and output of the mapping algorithm. A global grid (or universal grid) is defined as a two-dimensional regular grid with a user-defined origin and discretized LTP coordinates east and north (Rovira-Más, 2012). In reality, global grids are the quantization of the LTP coordinate system as a means to manage crop production information at a global scale; allowing the exchange of information among successive seasons and the comparison of multiple parameters on the same field. Figure 5 schematizes the process to create global grid maps from LTP coordinates. The first stage in the construction of the map consists of establishing its boundaries according to the extreme east (E) and north (N) coordinates, as labeled in the conceptual plot of Figure 5 (*minE*, *maxE*, *minN*, *maxN*). Once the map limits have been set and the size of the square cell (*c*) has been chosen, the cell of the grid corresponding to any particular position of coordinate (E, N) can be calculated with Equation (5) and Equation (6). As the resolution of the global grid directly depends on the user-selected size of the cell, therefore, changing the size of the cell will necessarily lead to a change in resolution. The resolution of the global grid is determined by the level of detail required by each application. The positions of the cells in the grid are numbered in the same fashion as matrices, and as a result the discrete coordinates of the grids *x* and *y* are non-negative integers. Equation 5 and Equation 6 yield the position of the cell for point *k*, where the original LTP coordinates are ($E(k)$, $N(k)$), the size of the cell is *c*, and the global grid coordinates are ($x(k)$, $y(k)$). The coordinates min*E* and min*N* are the minimum values of coordinates east and north, respectively.

$$x(k)=\frac{\min E+E}{c};\ c\in\mathbb{N};\ c>0 \tag{5}$$

$$y(k)=\frac{N-\min N}{c};\ c\in\mathbb{N};\ c>0 \tag{6}$$

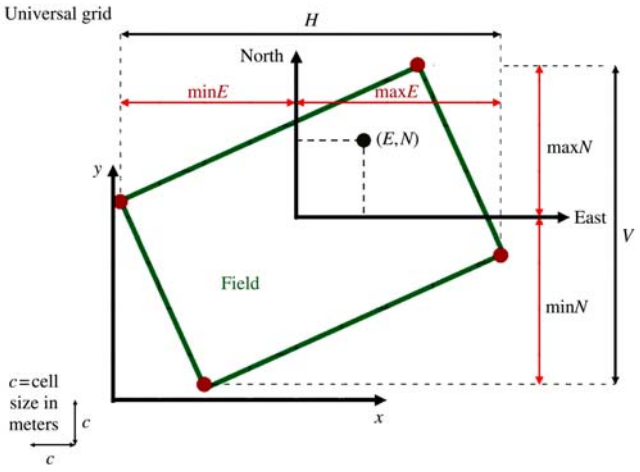

Figure 5 Transformation from LTP coordinates to global grid cells

When different global maps representing the same vineyard need to be compared, it is a good practice to maintain the same resolution, i. e. the same cell dimension, for all the maps; however, enlarging the size of the cells may result in a loss of information. The

cells of global grids were filled-in according to the data recorded by the perception and localization algorithms. Each percentage of vegetation was taken to the cells calculated with Equation (5) and Equation (6) after introducing the LTP coordinates associated with each image. When a given cell was already filled with a percentage of vegetation and new information became available for that particular cell, the algorithm updated the cell with the average value of old and new data.

With the purpose of controlling the perception and localization algorithms efficiently, which had to run in the computer aboard in real time, the customized interface of Figure 6 was designed. This graphic user interface (GUI) allowed the visualization of the three key images related to vigor quantification: the original image acquired by the NIR-filtered camera (Figure 6a), the segmentation profile with its corresponding automatic threshold μ (Figure 6b), and the segmented image after applying either the automatic or the manual threshold (Figure 6c). Together with image supervision, the quality of GPS data was continuously tracked too, as only images with acceptable coordinates were added to the vigor maps. This graphic interface allowed the user to set the working requirements for the minimum number of satellites and maximum magnitude of the Horizontal Dilution of Precision (HDOP).

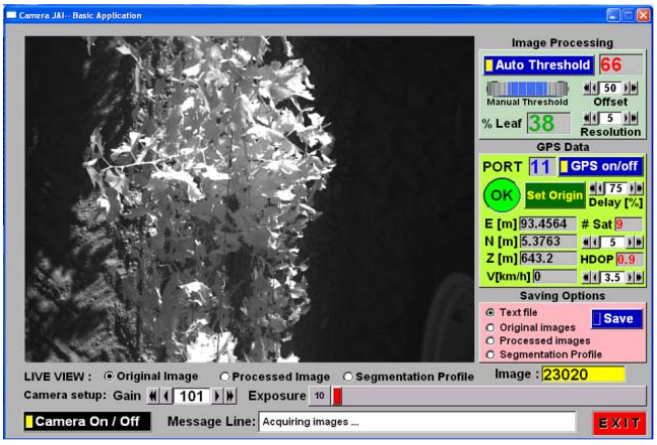

a. NIR-filtered image

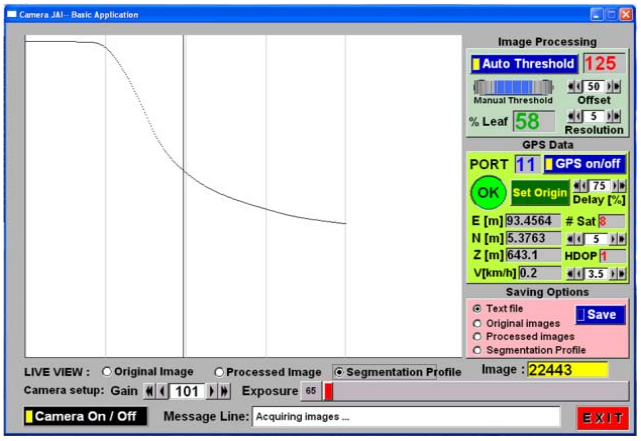

b. Segmentation profile curve and automatic threshold

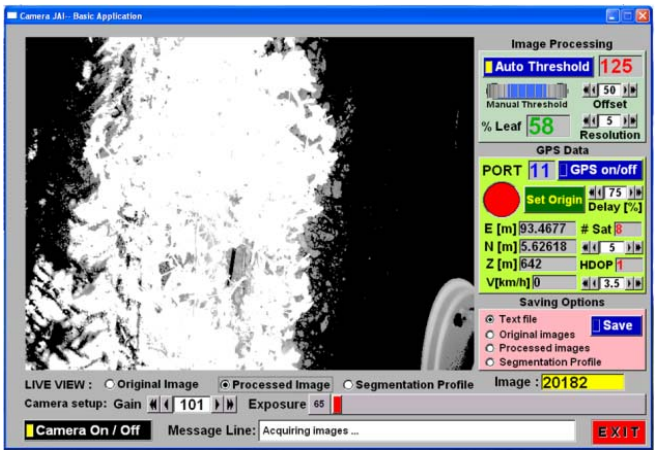

c. Segmented image

Figure 6 Control interface for vigor map construction

Since vigor has been traditionally correlated to yield, yield maps may be resourceful to validate the information contained in grid-based vigor maps. The harvester used in the field where the tests took place was not equipped with a yield monitor, and consequently grapes had to be manually harvested in order to build a yield map. Grapes were weighted with a dynamometer (Compact Force Gauge, Mecmesin, West Sussex, UK) every trellis post, which practically corresponded to a weight measurement every six meters along the vehicle path

delimited by rows one to eight. The locations at which grapes were weighted were also globally referenced with the StarFire™ GPS receiver, establishing a unique common origin for all vigor maps and the yield map used in the validation. The procedure to build the yield map was exactly the same used to create vigor maps (Equation (5) and Equation (6); Figure 5), but instead of filling the cells with image-based vigor estimates, cells were occupied by the weight of grapes manually harvested in the field. The yield map used to evaluate vigor maps was assembled after weighting grapes at the 113 points marked along the six passes traced in Figure 7a. These points were positioned with the StarFire™ GPS and transformed to LTP coordinates. The yield associated to each of the 113 sampled points corresponded to a length of about six meters of trellised vines located on the left side of the vehicle, keeping the same geometrical relationship between vehicle path and sensed canopy used during image acquisition. In order to ease the comparison between yield and vigor maps, all the maps were normalized by setting a square cell size of 5 m side, resulting in regular squares of 25 m^2 carrying the average yield or vigor associated to the points falling inside each cell.

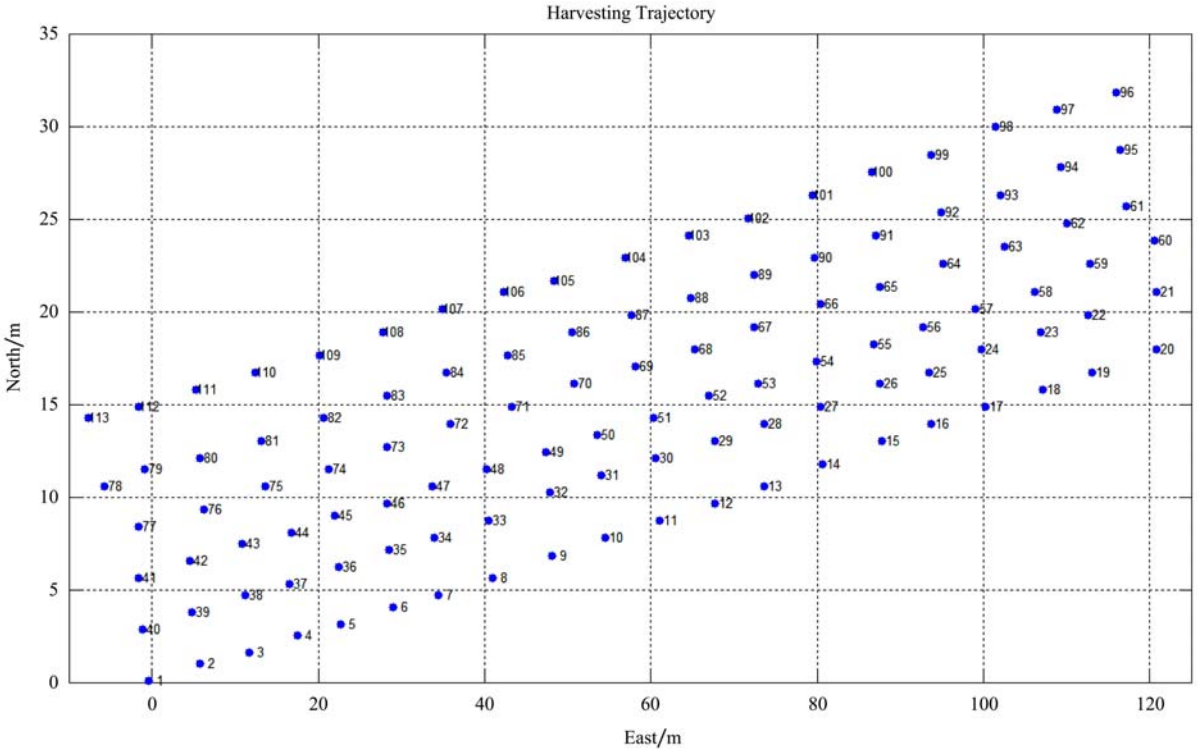

a. Generating points

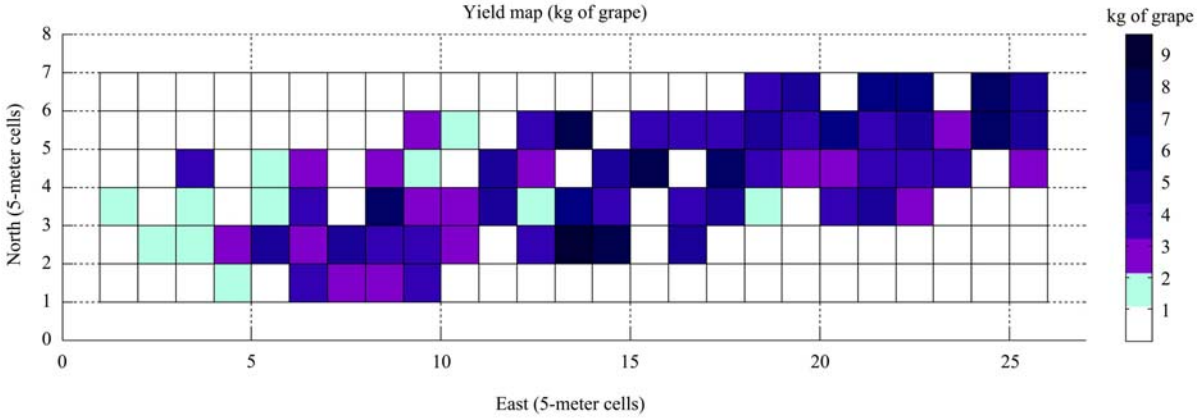

b. Final map

Figure 7 Grid-based yield map

3 Results and discussion

The complete yield map generated from the 113 points of Figure 7a is plotted in Figure 7b, and it shows variability in yield, as expected. In particular, the initial 30 m in the east side of the field indicates a considerable low yield in comparison to the rest. The main reason for these differences in yield was a disadvantageous slope (3% in average) in the terrain that reduces the quantity of water available for the vines in this location. In addition to internal differences due to water availability, the entire field was severely attacked by powdery mildew (*Plasmopara viticola*), which accounted for the low yield rates averagely measured. The half field in the east side (right side in the grid) was situated at the lowest elevation of the farm, and water generally accumulated towards the eastern headlands, resulting in cells with higher yield rates. Furthermore, the damage caused by mildew was apparently less severe in the east section of the field.

Figure 8 shows a vigor map generated from NIR images taken along rows 2, 3, 6, and 7. The rest of the rows tested are not included in the map due to the reception of incorrect or unreliable GPS messages. According to the vigor map depicted in Figure 8, the spatial distribution of vine vigor, here quantified as percentage of healthy vegetation, clearly shows a concentration of weaker plants in the west side of the field, which is in accordance with the lower yield rated for the same area as indicated by Figure 7b. Notice the advantages of normalizing the resolution of the maps with cells of equal dimensions, as cell-to-cell correlations may be calculated between yield and vegetation. The automatic estimation of vegetation from zenithal images leads to several measurements within the same cell, as a consequence of sampling rate, camera field of view, and vehicle forward speed. The final value represented in each cell was the average of all the values associated to that cell. The statistical analysis of correlating every cell of Figure 8 with its corresponding cell of Figure 7b led to the model of Equation (7), where Y represents the yield per cell in kg and V is the relative vegetation in percentage. This result, graphically represented in Figure 9, confirms that there exists statistical significance with a 99% confidence level, where the model explains 39.9% of the variability in yield. On the whole, the deepest part of the field resulted in both higher yield and vigor, something already noticed by Johnson et al. (2001) in the study of irrigation management based on remote sensing for commercial vineyards in Napa Valley, California.

$$Y\,(\text{kg/cell}) = 0.465172 + 0.065518 \cdot V\,(\%) \qquad (7)$$

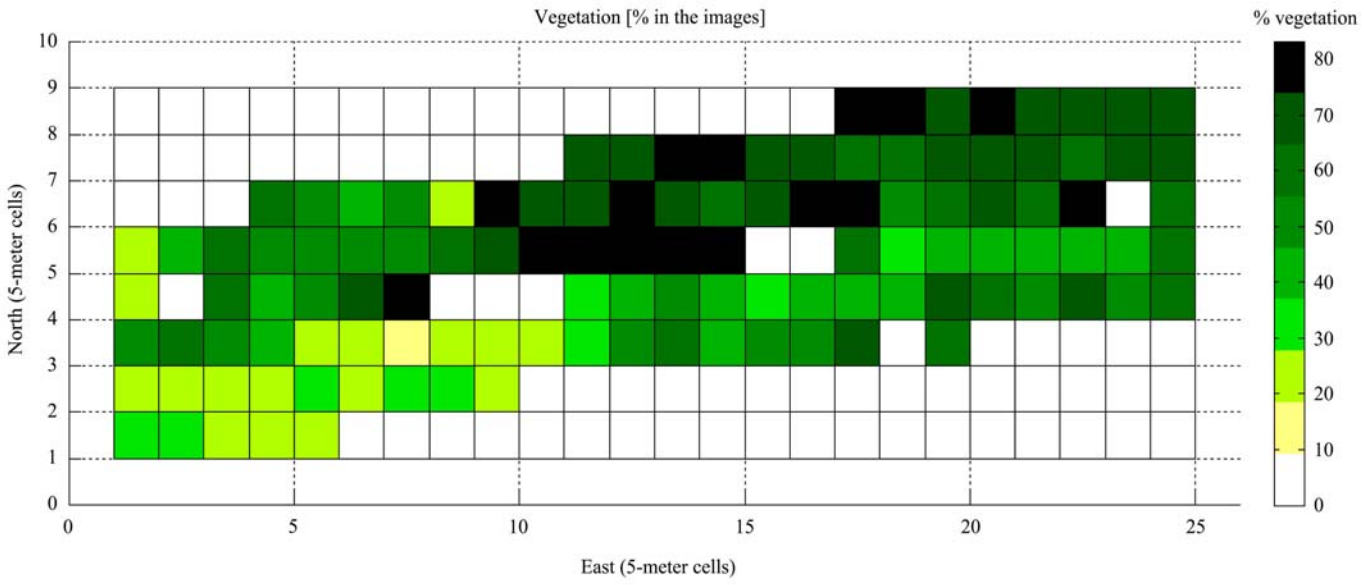

Figure 8 Grid-based vigor map from NIR images acquired on rows 2, 3, 6, and 7

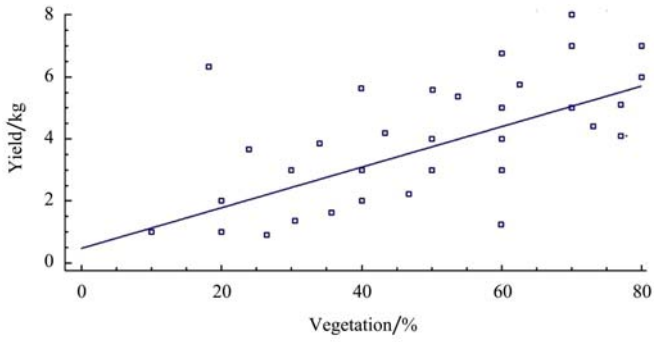

Figure 9 Correlation model between NIR-based vegetation (%) and grape yield (kg cell^{-1})

The analysis of various series of images taken with the camera located at different positions in the vehicle demonstrated that zenithal images, i. e. those providing a top view, gave the best results in terms of vigor quantification. Nevertheless, some field scenes with adverse illumination occasionally resulted in challenging images to be thresholded in automatic mode. Figure 10a, for instance, is a typical image correctly segmented by the algorithm. It shows a top view of the vine where everything that is not vegetation, including the wires of the supporting structure, has been eliminated. In these segmented images, non-black pixels are valid indicators of vigorous vegetation, and the percentage of non-black pixels in the image gives an estimate of the relative amount of vegetation for a precise location in the field, an indirect assessment of the vigor of the plants. On the other hand, Figure 10b shows a problematic image in which the strong sun at noon enhanced the reflectance of the soil, complicating the isolation of vegetation.

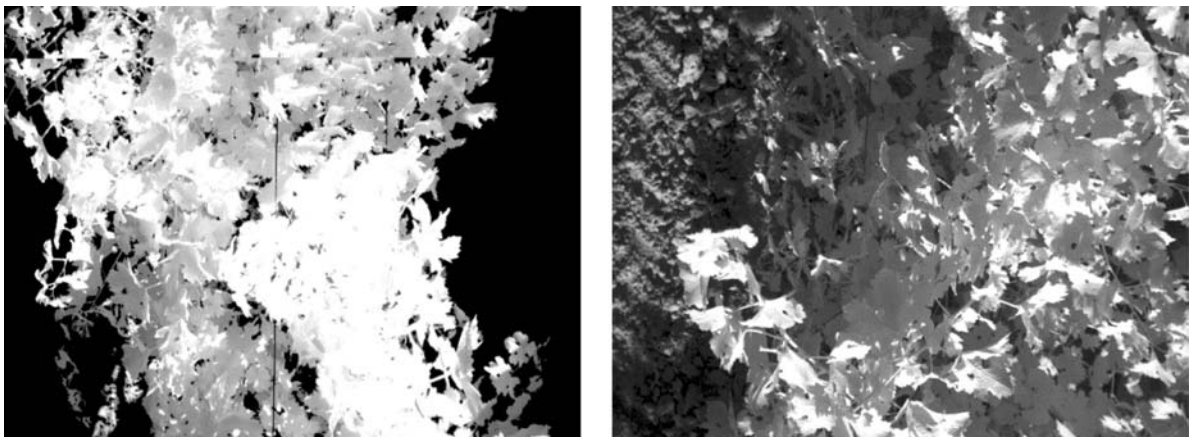

a. Correct segmentation b. Soil-induced errors

Figure 10 Automatic segmentation results

Even though field results showed the superiority of zenithal images to lateral images for vigor mapping, there exist alternative studies that give preference to lateral views for proximal sensing of vineyard variability (Bramley et al., 2007). Lateral images are defined as the images captured with the camera facing one of the sides of the continuous row in such a way that the sensor array of the camera is approximately parallel to the canopy and perpendicular to the moving direction (Figure 11a). Due to important disadvantages found in the field with lateral images, the prototype proposed for vigor mapping only used zenithal images. To begin with, placing the camera between fully-grown rows of vines at plant height resulted in too small - sometimes inexistent - separation between camera and plants, which produced weak images for quantifying differences in vigor, and eventually was the cause of a broken camera. In addition, the detection algorithm failed when the row being sensed had patches of no vegetation, as contiguous rows fooled the system, which assigned vegetation to places with no vines (Figure 11a). These false positives were the reason to assign higher vigor values to sections of the field with meager vines, as in the vigor map of figure 11b which shows vigorous plants in the west side of the field. This serious problem has been dodged in the past by affixing a large screen to the vehicle in such a way that the background of the image was always controlled (Praat et al., 2004). However, such a cumbersome and bulky solution opposes one of the central objectives of this research, which intends to configure a system easy to

integrate in conventional vehicles, as the one shown in Figure 1, to avoid rejection by farmers and producers in search for effective solutions at minimum cost and the lowest possible complexity. The flexibility pursued with this system also affects the capacity of users to adjust the cost of hardware according to the precision required, as there exist GPS receivers of practically any price, vision sensors range from inexpensive webcams to high performance cameras, and any moderate quality computer suffices to run the proposed software.

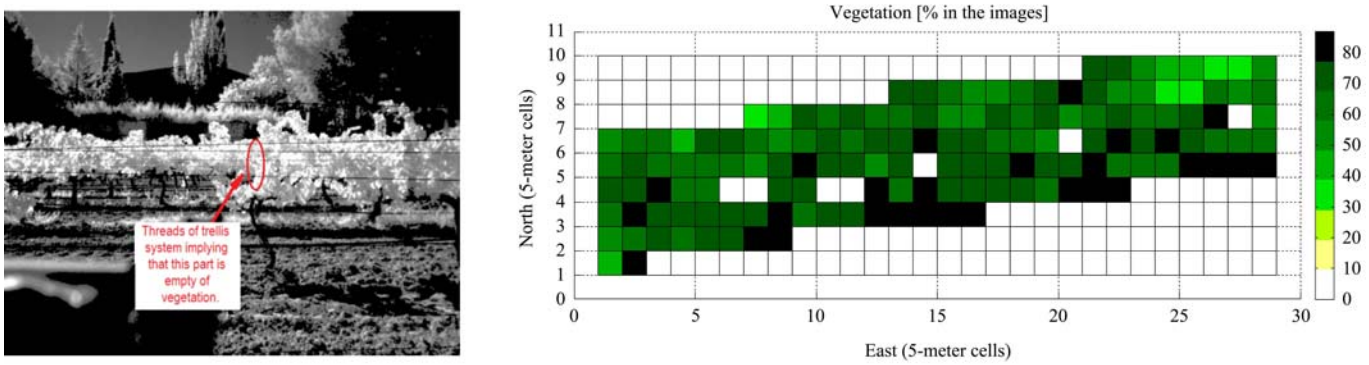

a. Undetected gaps

b. Consequential defective vigor maps

Figure 11 Lateral sensing

4 Conclusion

Once technology has been proved useful and helpful to assist producers in the management of their fields, only applications with easy access, simple means of adoption, and reasonable cost will have potential in the near future. The ground-based sensing system proposed in this article is meant to be incorporated to conventional vehicles, and provides an estimate of the spatial variation of vine vigor in a global grid format. Vigor differences have been correlated to yield variability, and as a result vigor maps can be used as a predictive tool for farmers. The grid-based global maps developed for this project facilitate the rapid exchange of crop information and favors the comparison of vigor maps with other maps of alternative production parameters. Field tests confirmed the superiority of zenithal images to side views, which led to establish a direct correlation between estimated vigor and measured yield. However, more robustness needs to be added to the perception algorithm in order to improve its performance under adverse illumination conditions, especially by reducing the confusing effect of soil reflectance. Reliability must also be strengthened in terms of GPS vehicle positioning, as the real time integration of image acquisition and GPS message conditioning sometimes jammed the onboard computer and delayed the construction of the maps. In conclusion, the methodology proposed opens a field of austere applications which sacrifice certain complexity in order to gain accessibility by the end users who, in the end, need to improve their management with the least investment.

Acknowledgements

The authors would like to express their gratitude to Luis Gil-Orozco Esteve from the winery and vineyards Finca Ardal, and to Miguel Ricau Ibáñez, owner of two traditional vineyards where experimental testing took place. We also thank Montano Pérez Teruel and Juan José Peña Suárez for the preparation of the experimental vehicle, especially the supporting frames and wiring of the camera. The corporation Edmund Optics deserves special appreciation for providing technical material through the *Third European Prize 2011* within the *2011 Research and Innovation Award*. In addition, we are also grateful to the city of Valencia (Spain) for the concession of the award *Valencia Idea 2011* to this research project.

Nomenclature

h 8-bit grey level (gray level)

$P(h)$ Segmentation profile. Percentage of pixels in the

image with grey level superior to h (%)

∇ Gradient

$\Delta(h)$ Estimation of the gradient for intensity level h

∇ Curvature

$\Delta^2(h)$ Estimation of the curvature for intensity level h

δ Resolution. Finite interval considered for gradient and curvature calculations (gray level)

λ Offset (gray level)

h_Δ Grey level that maximizes $\Delta(h)$ (gray level)

$h_{\Delta 2}$ Grey level that maximizes $\Delta^2(h)$ (gray level)

μ Dynamic threshold (gray level)

References

Alchanatis, V., Y. Cohen, S. Cohen, M. Moller, M. Meron, J. Tsipris, V. Orlov, A. Naor, and Z. Charit. 2006. Fusion of IR and multispectral images in the visible range for empirical and model based mapping of crop water status. 2006 *ASAE* Annual Meeting, paper No. 061171.

Baluja, J., M.P. Diago, P. Groovaerts, and J. Tardáguila. 2012. Assessment of the spatial variability of anthocyanins in grapes using a fluorescence sensor: relationships with vine vigour and yield. *Precision Agriculture*, 13: 457-472.

Best, S., L. León, F. Flores, H. Aguilera, R. Quintana, and V. Concha. 2011. *Handbook. Agricultura de Precisión*. Progap – INIA Programa de Agricultura de Precisión. http://www.elsitioagricola.com/CultivosExtensivos/LibroIniaAP/libro3.asp [In Spanish] (Accessed on 11/01/2012)

Blackmore, S. 2000. Using information technology to improve crop management, February 29, 2000: *Weather Agro-Environmental Management.* Dublin, AgMet Millennium.

Bramley, R., and S. Williams. 2001. A protocol for the construction of yield maps from data collected using commercially available grape yield monitors. http:www.cse.csiro.au/client_serv/resources/CRCVYield_Mapping_Protocol.pdf (Accessed 1 December, 2011)

Bramley, R., D. Gobbet, and J. P. Praat. 2007. A proximal canopy sensor - A tool for managing vineyard variability and adding value to viticultural research. *Grape and wine research and development corporation.* Final report. Project number CSL 06/01 July 2007.

Bramley, R. G. V., J. Ouzman, and C. Thornton. 2011a. Selective harvesting is a feasible and profitable strategy even when grape and wine production is geared towards large fermentation volumes. *Australian Journal of Grape and Wine Research,* 17(3): 298-305.

Bramley, R., M. Le Moigne, S. Evain, J. Ouzman, L. Florin, E. Fadaili, C. Hinze, and Z. Cerovic. 2011b. On-the-go sensing of grape berry anthocyanins during commercial harvest: development and prospects. *Australian Journal of Grape and Wine Research,* 17: 316-326.

Bramley, R., M.C.T. Trought, and J. P. Praat. 2011c. Vineyard variability in Marlborough, New Zealand: characterising variation in vineyard performance and options for the implementation of Precision Viticulture. *Australian Journal of Grape and Wine Research,* 17: 72-78.

Chaerle, L., and D. Van Der Straeten. 2000. Imaging techniques and the early detection of plant stress. *Trends in plant science,* 5(11): 495-501.

Eklundh, L., H. Jin, P. Schubert, R. Guzinski, and M. Heliasz. 2011. An optical sensor network for vegetation phenology monitoring and satellite data calibration. *Sensors,* 11: 7678 - 7709.

Gausman, H. W. 1977. Reflectance of leaf components. *Remote Sensing of Environment,* 6:1-9.

Giles, K., and D. Downey. 2001. Quality control verification and mapping system for chemical application. *ASAE* Paper No. 01-1049.

Godwin, R. J., and P. C. H. Miller. 2003. A review of the technologies for mapping within-field variability. *Biosystems Engineering,* 84(4): 393-407.

Grewal, M. S., L. R. Weill, and A. P. Andrews. 2001. *Global Positioning Systems, Inertial Navigation, and Integration*. John Wiley Sons, New York.

Hall, A., D. W. Lamb, B. Holzapfel, and J. Louis. 2002. Optical remote sensing applications in viticulture - a review. *Australian Journal of Grape and Wine Research,* 8(1): 36 - 47.

Johnson, L. F., R. R. Nemani, L. L. Pierce, M. R. Bobo, and D. Bosch. 2000. Toward the improved use of remote sensing and process modeling in California's premium wine industry. International Geoscience and Remote Sensing Symposium, pp. 363–365.

Johnson, L.F., Bosch, D. F., Williams, D.C., and Lobitz, B.M. 2001. Remote sensing of vineyard management zones: implications for wine quality. *Applied Engineering in Agriculture,* 17(4): 557-560.

Johnson, L. F., E. Roczen, S. K. Youkhana, R. R. Nemani, and D. F. Bosch. 2003. Mapping vineyard leaf area with multispectral satellite imagery. *Computers and Electronics in Agriculture,* 38(1): 33-44.

Kim, Y., J. F. Reid, A. Hansen, Q. Zhang, and M. Dickson. 2001.

Ambient Illumination effect on a spectral image sensor for detecting crop nitrogen stress. *ASAE* Paper 011178.

Kimes, D. S. 1983. Dynamics of directional reflectance factor distributions for vegetation canopies. *Applied Optics,* 22(9):1364-1372.

Knipling, E. B. 1970. Physical and physiological basis for the reflectance of visible and near-infrared radiation from vegetation. *Remote Sensing of Environment,* 1(9): 155-159.

Lacar, F. M., M. M. Lewis, and I. T. Grierson. 2001. Use of hyperspectral imagery for mapping grape varieties in the Barossa Valley, South Australia. *Transactions International Geoscience and Remote Sensing Symposium. 3-13 June 2001, Sydney, Australia, 2001.*

Lamb, D., A. Hall, and J. Louis. 2001. Airborne remote sensing of vines for canopy variability and productivity. *The Australian Grapegrower and Winemaker,* 449a: 89-92.

Lamb, D. W., M. M. Weedon, and R. Bramley. 2004. Using remote sensing to predict grape phenolics and color at harvest in a Cabernet Sauvignon vineyard: timing observations against vine phenology and optimising image resolution. *Australian Journal of Grape and Wine Research,* 10(1): 46-54.

McCarthy, C.L., N. H. Hancock, and S. R. Raine. 2010. Applied machine vision of plants - A review with implications for field deployment in automated farming operations. *Intelligent Service Robotics,* 3(4): 209-217.

Noh, H., Q. Zhang, S. Han, B. Shin, and D. Reum. 2005. Dynamic calibration and image segmentation methods for multispectral imaging crop Nitrogen deficiency sensors. *Transactions of the ASABE,* 48(1): 393-401.

Praat, J., F. Bollen, and K. Irie. 2004. New approaches to the management of vineyard variability in New Zealand. *12th Aust. Wine Ind. Tech. Managing Vineyard Variation* (precision viticulture), pp 24–30.

Rovira-Más, F. 2010. Sensor architecture and task classification for agricultural vehicles and environments. *Sensors,* 10(12): 11226-11247.

Rovira-Más, F., Q. Zhang, and A. C. Hansen. 2011. *Mechatronics and Intelligent Systems for Off-road Vehicles*. Springer-Verlag, London.

Rovira-Más, F., and R. Banerjee. 2012. GPS data conditioning for enhancing reliability of automated off-road vehicles. *Journal of Automobile Engineering*. Electronic version DOI: 10.1177/0954407012454976.

Rovira-Más, F. 2012. Global-referenced navigation grids for off-road vehicles and environments. *Robotics and Autonomous Systems,* 60(2): 278-287.

Sáiz-Rubio, V., and F. Rovira-Más. 2012. Dynamic segmentation to estimate vine vigor from ground images. *Spanish Journal of Agricultural Research*, 10 (3): 596-604.

Schopfer, J., S. Huber, D. Odermatt, T. Schneider, W. Dorigo, N. Oppelt, B. Koetz, M. Kneubuehler, and K. I. Itten. 2007. Towards a comparison of spaceborne and ground-based spectrodirectional reflectance data. *'Envisat Symposium 2007'*, (ESA SP-636, July 2007, 23–27 April, Montreux, Switzerland.

Taylor, J., B. Tisseyre, and J. P. Praat. 2005. Bottling Good Information: Mixing Tradition and Technology in vineyards Information and Technology for Sustainable Fruit and Vegetable Production. FRUTIC 05. Sept 2005, Montpellier, France.

Weekley, J. G. 2007. Multispectral imaging techniques for monitoring vegetative growth and health. Master thesis. Virginia Polytechnic Institute and State University. Virginia, USA.